Improved *in situ* Sr isotopic analysis by a 257 nm femtosecond laser in combination with the addition of nitrogen for geological minerals

Wen Zhang[a], Zhaochu Hu[a,*], Yongsheng Liu[a], Tao Wu[b], Xiaodong Deng[a], Jingliang Guo[a], Han Zhao[a]

[a] *State Key Laboratory of Geological Processes and Mineral Resources, China University of Geosciences, Wuhan 430074, China*
[b] *School of Earth Sciences, Zhejiang University, Hangzhou 310027, China*

ARTICLE INFO

ABSTRACT

In situ Sr isotope analysis of geological materials by laser ablation multiple collector-inductively coupled plasma mass spectrometry (LA-MC-ICP-MS) is a powerful tracer technique for tracking magmatic source components and geological processes. However, the accuracy and precision of the $^{87}Sr/^{86}Sr$ ratio are limited in the analysis of natural minerals because of the low-Sr concentration, the isobaric interference or small grains with complex textural contexts, especially for transparent minerals such as feldspars. In this study, analytical results demonstrated that ablation rates in fs laser ablation were consistent for various samples (0.08–0.11 μm per pulse), but those in ns laser ablation were obviously material properties-dependent, such as the rates of 0.026 μm per pulse and 0.144 μm per pulse for feldspar and pyrite, respectively. In addition, at similar energy fluences, the sensitivities of Sr in feldspars analyzed by the fs laser were 3.4 times higher than those analyzed by the ns laser due to the higher ablation efficiency of the fs pulse. These advantages of the fs laser not only offer the benefit of eliminating or weakening the matrix effect during the laser ablation processes but also help to improve the analytical precision for transparent minerals. We also demonstrated that the isobaric interferences of calcium dimers and argides ($CaAr^+ + CaCa^+$) and Kr^+ were dramatically reduced by factors of 6.5–11.7 and 5–12.5 in the presence of 6–12 ml min^{-1} N_2, respectively. Furthermore, with the addition of N_2 (12 ml min^{-1}), the sensitivity of Rb was inhibited, resulting in a decrease of 1.47 times in Rb/Sr signal ratios. Due to the effect of suppressing interferences by adding N_2, both the stability and accuracy of the $^{87}Sr/^{86}Sr$ and $^{84}Sr/^{86}Sr$ ratios show improvement, especially for the Rb-rich feldspars.

Combining the advantages of the fs laser system with the addition of nitrogen, an improved *in situ* Sr isotope analytical method is then developed. The satisfactory accuracy and precision of the $^{87}Sr/^{86}Sr$ ratio from natural plagioclases, a K-feldspar with high Rb/Sr ratios (0.46) and a low-Sr clinopyroxene were obtained, demonstrating the reliability of the proposed method. Four feldspars, which have different contents of the major elements, Sr and Rb, showed homogeneous Sr isotope compositions and were recommended as potential suitable reference materials for *in situ* Sr isotope analysis. As an application, two plagioclases in mafic microgranular enclaves (MMEs) with small grain sizes (200–300 μm) and wide ranges of Rb/Sr ratios were analyzed and showed obvious variations of the $^{87}Sr/^{86}Sr$ ratios from core to rim, which indicated that the proposed method in this study can provide high spatial resolution geochemical information for a single mineral.

1. Introduction

The radiogenic $^{87}Sr/^{86}Sr$ ratio is an important geochemical tracer in solid earth sciences (Davidson et al., 2001; Jackson and Hart, 2006). High precision and bulk-rock Sr isotopic ratios have been determined mainly by thermal ionization mass spectrometry (TIMS) (Yang et al., 2010; Koornneef et al., 2015) and multiple collector-inductively coupled plasma mass spectrometry (MC-ICP-MS) (Waight et al., 2002;

Galler et al., 2007; Yang et al., 2011a). However, bulk-rock Sr isotopic ratios generally reflect a mixed signature of various end-members that might not reach isotope equilibrium in the targeted rock (Davidson et al., 2001; Davidson et al., 2007; Ramos and Tepley, 2008). In this regard, *in situ* Sr isotopic measurements using laser ablation (LA)-MC-ICP-MS offer the spatial resolution to identify and distinguish the inter- and intra-crystalline isotopic variations of mineral grains on the scale of tens of microns. As a result, LA-MC-ICP-MS for Sr isotopic

measurements has received increasing interest in earth science, environmental science and archaeology applications, including: (1) magmatic minerals such as carbonate, apatite, plagioclase, clinopyroxene, and perovskite (Christensen et al., 1995; Davidson et al., 2001; Waight et al., 2002; Bizzarro et al., 2003; Schmidberger et al., 2003; Ramos et al., 2004; Woodhead et al., 2005; Yang et al., 2009; Kimura et al., 2013; Tong et al., 2016) and melt inclusion (Jackson and Hart, 2006); (2) biogenic carbonate such as otoliths (Outridge et al., 2002; Barnettjohnson et al., 2005) and shells (Christensen et al., 1995; Ramos et al., 2004; Horstwood et al., 2008); and (3) archaeological tooth enamel (Balter et al., 2008; Copeland et al., 2010).

Christensen et al. (1995) first demonstrated the feasibility of *in situ* Sr isotopic analysis using LA-MC-ICP-MS on both carbonate and feldspar samples. Further studies reported highly precise (30–100 ppm) and accurate $^{87}Sr/^{86}Sr$ isotope ratios with the nanosecond (ns) laser ablation system (Davidson et al., 2001; Waight et al., 2002; Ramos and Tepley, 2008; Kimura et al., 2013; Chen et al., 2015). Most of interesting and measured minerals for *in situ* Sr isotopic analysis were transparent minerals. The previous studies reported that the interaction between transparent minerals and ns laser pulses was a non-linear absorption process known as avalanche ionization (Liu et al., 1997; Shaheen et al., 2012). In this process, ablating transparent materials by ns laser pulses depends on the pre-existence of seed electrons, which are metallic impurities or thermal ionizations of shallow energy levels in the transparent materials used to initiate laser-induced breakdown. However, the seed electrons are normally only present at low concentrations and are randomly distributed in transparent materials, resulting in stochastic and inefficient ablation behavior (Liu et al., 1997). In the previous studies, therefore, large spot sizes (100–300 μm) were required to obtain sufficient signal intensity for $^{87}Sr/^{86}Sr$ isotopic analyses of geological samples.

Recently, femtosecond (fs) laser ablation systems with short pulse widths have become available (Russo et al., 2002; Hergenröder et al., 2006; Fernández et al., 2007; Pisonero and Günther, 2008; Shaheen et al., 2012). With fs laser ablation, the pulse duration (< 1 ps) is shorter than the phonon relaxation time (*ca.* 10 ps) (von der Linde et al., 1997; Mao et al., 2004). Ultrafast energy deposition with fs laser pulses vaporizes and ablates the illuminated volume before thermal relaxation sets in. The heat diffusion, which occurs during the ns laser pulse and results in a significant heat affected zone, is significantly inhibited (von der Linde et al., 1997; Mao et al., 2004). In addition, the pulse intensity (irradiance or power density) reaches much larger values for fs pulses ($10^{14}–10^{15}$ W cm^{-2}) compared to ns pulses ($10^9–10^{10}$ W cm^{-2}), which would improve the analytical quality of ablated materials. Due to these advantages, fs-LA-ICP-MS has been successfully applied to the analyses of element ratios and element concentrations (Poitrasson et al., 2003; Bian et al., 2006; Koch et al., 2006; Horn and von Blanckenburg, 2007; Borisova et al., 2008; Jochum et al., 2014; Li et al., 2015; Li et al., 2016) as well as isotope ratios, such as Sr (Campos-Alvarez et al., 2010; Yang et al., 2011b), U−Pb (Freydier et al., 2008; Hirata and Kon, 2008; Kimura et al., 2014), Pb (Shaheen and Fryer, 2010; Chen et al., 2014; Ohata et al., 2015), Mg (Oeser et al., 2014), Si (Chmeleff et al., 2008; Steinhoefel et al., 2011; Schuessler and von Blanckenburg, 2014), Fe (Horn et al., 2006; Steinhoefel et al., 2009b; Steinhoefel et al., 2009a; Oeser et al., 2014), and Cu (Ikehata et al., 2008; Ikehata and Hirata, 2013). However, the detailed studies for ablating transparent minerals by fs laser are not sufficient. There is great potential in elemental quantitative and isotopic ratio analyses with high spatial resolution for transparent minerals using a fs laser system.

An additional challenge for Sr isotope analysis using LA sampling is the variety of isobaric interferences on the Sr isotope spectrum, including Rb, Kr, doubly charged rare earth elements (REEs), calcium dimers and argides and possibly oxides (Ramos et al., 2004; Woodhead et al., 2005; Vroon et al., 2008; Yang et al., 2011b; Kimura et al., 2013; Yang et al., 2014). The strategies of eliminating or reducing these

isobaric interferences have been widely explored and still attract significant attention. In recent decades, mixed-gas plasma has been extensively investigated to overcome analytical limitations of the Ar plasma, including the addition of nitrogen (N_2), hydrogen (H_2), methane, carbon-containing solvents and water (Durrant, 1994; Guillong and Heinrich, 2007; Hu et al., 2008; Fliegel et al., 2011; Hu et al., 2012a; Shaheen et al., 2012; Lin et al., 2014; Liu et al., 2014; Xu et al., 2015; Fu et al., 2016; Tong et al., 2016). N_2 is one of the most widely used molecular gases in ICP-MS and has been utilized mainly for the improvement of sensitivity and stability, the decrease in polyatomic interferences and the attenuation of matrix effects. Recent studies show that adding N_2 to the Ar carrier gas can significantly enhance signal intensity during LA-MC-ICP-MS analysis, such as for Hf, Nd and Pb (Hu et al., 2012a; Shaheen et al., 2012; Xu et al., 2015). The N_2-related intensity enhancement was attributed to the higher thermal conductivity of N_2, which results in higher plasma temperature and the increased excitation and ionization efficiency of many elements (Hu et al., 2012a; Shaheen et al., 2012). However, the suppression of signal intensity resulting from N_2 addition has been observed in some analyses of B, S and Sr (Lin et al., 2014; Fu et al., 2016; Tong et al., 2016). Thus, the enhancement or suppression of signal intensity caused by the N_2 addition is element-specific. On the other hand, the more conclusive observation is that the addition of N_2 can reduce polyatomic interferences in the ICP. For example, Durrant (1994) first reported that the addition of approximately 1% (v/v) N_2 to the coolant flow or the addition of approximately 12% N_2 to the cell gas reduced CeO^+/Ce^+ and ThO^+/Th^+ ratios by a factor of 2–3 in LA-ICP-MS. Hu et al. (2008) noted that the addition of 5–10 ml min^{-1} N_2 to the central channel gas in LA-ICP-MS increased the sensitivity for most of the 65 investigated elements by a factor of 2–3 while reducing the oxide ratios (ThO^+/Th^+) (by one order of magnitude) and the hydride ratio (ArH^+/Ar^+) (by a factor of 3). Shaheen et al. (2012) showed increased abundances of doubly charged ions (U^{++}/U and Ce^{++}/Ce) but reduced oxide ratios (UO^+/U^+ and ThO^+/Th^+) and mass bias of Pb and Tl upon the addition of 5 ml min^{-1} N_2. Fu et al. (2016) reported that the addition of N_2 efficiently reduces polyatomic interferences (OO^+, SH^+ and OOH^+) for *in situ* S isotope analyses in sulfides.

Feldspars have high Sr abundances, ubiquitously occur in igneous rocks and exhibit a large range of crystallization temperatures (Gagnevin et al., 2005; Charlier et al., 2006; Davidson et al., 2007). Therefore, feldspars were selected in this study as the main research mineral for *in situ* Sr isotope analysis. Comparisons of the ablation rates, elemental sensitivities and analytical precision of $^{87}Sr/^{86}Sr$ ratios between a 257 nm fs laser and a 193 nm ArF excimer ns laser were performed. In addition, we systematically investigated the effects and limitations of small amounts of N_2 mixed to the central channel gas flow of LA-MC-ICP-MS. The suppression of the sensitivities towards Rb and Kr and yields of polyatomic interferences were found with the addition of N_2. Combining the high ablation efficiency of the fs laser with the capacity of suppressing the interference factors by adding N_2, the improved *in situ* Sr isotopic analysis method using the 257 nm fs laser was established. The feasibility and flexibility of the proposed method were demonstrated by analyzing common plagioclases, K-feldspars with high Rb/Sr ratios and low-Sr clinopyroxenes.

2. Analytical procedure

2.1. Instrumentation

In situ Sr isotope analyses were performed on a Neptune Plus MC-ICP-MS (Thermo Fisher Scientific, Bremen, Germany) coupled with two laser ablation systems at the State Key Laboratory of Geological Processes and Mineral Resources (GPMR), China University of Geosciences (Wuhan), China. The Neptune Plus, a double focusing MC-ICP-MS, was equipped with seven fixed electron multiplier ICs, and nine Faraday cups fitted with 10^{11} Ω resistors. In addition, a large dry

Table 1
Summary of the operating parameters for the 193 nm excimer laser, the 257 nm fs laser, the MC-ICP-MS and the desolvation nebulizer system.

Cup-configuration	L4 ^{83}Kr	L3 ^{167}Er^{++}	L2 ^{84}Sr	L1 ^{85}Rb	C ^{86}Sr	H1 ^{173}Yb^{++}	H2 ^{87}Sr	H3 ^{88}Sr
RF Power				1250 W				
Cool gas flow				16.0 L min^1				
Auxiliary gas flow				0.10 L min^1				
Argon make-up gas flow				0.80 L min^1				
Helium carrier gas flow				0.50 L min^1				
Nitrogen gas flow				0, 6, 12 ml min^1				
Interface cones				X skimmer cone + Jet sample cone				
Instrument resolution				~ 400 (low)				
Block number				1				
Cycles of each block				160				
Integration Time (s)				0.524 sec.				
Laser ablation system								
Laser type		ArF excimer laser				Yb:YAG femtosecond laser		
Wavelength		193 nm				257 nm		
Pulse length		15 ns				300 fs		
Energy density		2.3-13.3 J cm^2				0.50-3.85 J cm^2		
Spot size		60, 90.120 μm				45, 60 μm		
Laser frequency		10 Hz				10-200 Hz		
Line scanning rate		-				5 μm s^1		
Aridus Ⅱ desolvation nebuliser system								
Membrane temperature				160 ℃				
Spray chamber temperature				110 ℃				
Sweep gas flow				2.5 L min^1 Ar				
Sample uptake rate				50 μL min^1 PFA nebuliser				
Nebuliser flow				0.95 L min^1				

interface pump (120 m^3 hr^{-1} pumping speed) and a newly designed X skimmer cone and Jet sample cone were used to increase the instrumental sensitivity. The Faraday collector configuration of the mass system was composed of an array from L4 to H3 to monitor Kr, Rb, Er, Yb and Sr (Table 1). Two different laser systems were used: a GeoLas 2005 system (Lambda Physik, Göttingen, Germany), which consisted of a COMPexPro 102 ArF excimer laser (Coherent Inc., Santa Clara, CA, U.S.A.) and a Microlas optical system; an NWR Femto^{UC} femtosecond system (New Wave Research, Fremont, CA, U.S.A.), which consisted of a 300 fs Yb:KGW femtosecond laser amplifier (PHAROS, Light Conversion Ltd., Vilnius, Lithuania) with a wavelength of 257 nm and ESI NWR Femto laser ablation system components. The laser ablation for both laser systems was conducted under a helium atmosphere in the same ablation cell (Geolas 2005) with a volume of *ca.* 40 cm^3, an inlet nozzle (i.d. < 0.5 mm) and a wide outlet (i.d. 1.5 mm), while argon was mixed into the sample-out line down-stream from the ablation chamber prior to entering the torch. To decrease the Tau effect (essentially a delay in the response of the resistors), a new signal-smoothing device (Hu et al., 2012b) was used downstream from the sample cell, which almost eliminated the short-term variability of the signal. Details of the instrumental operating conditions and measurement parameters are summarized in Table 1.

A LA-ICP-MS combination, consisting of an Agilent 7500a ICP-MS (Agilent Technology, Tokyo, Japan) coupled with the ns- or fs-laser ablation systems, was used for the measurements of major and trace element concentrations in natural minerals and reference glasses. Detailed operating conditions for the laser ablation system and the Q-ICP-MS instrument and data reduction are given in Supplementary Information A.

The CETAC Aridus II™ desolvation nebulizer system (CETAC Technologies, Omaha, USA) was used to investigate the influence of interferences on Sr isotopic determination. A series of NIST SRM 987 solutions doped with interfering elements were measured using MC-ICP-MS. The solutions were self-aspirated at an uptake of 100 ml min^{-1} through the PFA nebulizer and desolvated by the Aridus II system.

The Surface Profiler (P16$^+$, KLA-Tencor, California, USA) was used to measure the depth of the ablated crater. Each crater was profiled across the centerline over a range of 200 μm using a speed of 10 μm s^{-1}. The P16$^+$ Surface Profiler uses a diamond stylus (radius = 2 μm). Tests were performed at the Center of Micro-

Fabrication and Characterization (CMFC) of the Wuhan National Laboratory for Optoelectronics (WNLO), China.

2.2. Samples and reagents

The NIST reference glasses SRM 610 and SRM 612, USGS reference glasses BHVO-2G and GSE-1G and MPI-DING reference glasses ATHO-G, StHs6/80-G and T1-G were analyzed.

Three feldspar megacrysts, YG0440 (albite), YG0383 (albite) and YG4301 (anorthite), were collected from Hebei Province (China) and investigated in this study, A K-feldspar megacryst (Tuyk) from a pegmatite deposit in Henan province (China) with a high Rb/Sr ratio (0.46) was used. Feldspar megacrysts were crushed into 2–5 mm fragments and cleaned with deionized water. Some of the fragments were mounted in epoxy resin discs for elemental and Sr isotope analyses using LA-ICP-MS and LA-MC-ICP-MS, respectively. The remaining fragments were milled to < 200 mesh and were then acid-digested for Sr isotope ratio measurements by TIMS. A natural clinopyroxene megacryst (Cpx, HNB-8) with a low Sr concentration (89.2 μg g^{-1}) was analyzed. The chemical and Sr isotopic compositions of Cpx HNB-8 have been reported by He et al. (2013) and Tong et al. (2016).

Samples of natural pyrite and garnet from the Rock and Mineral Teaching Section in the China University of Geosciences (Wuhan) were used to investigate the difference in the laser rate between ns and fs laser ablation. Their chemical and isotope compositions were not determined.

A Sr isotope-certified reference material (NIST SRM 987) and a Rb isotope-certified reference material (NIST SRM 984) (NIST, Gaithersburg, USA) were prepared using 2% HNO$_3$. Single element standard solutions of Ca, Er and Yb (National Center for Analysis and Testing of Steel Materials, China) were used for the experiments with doped interfering elements. Commercially available nitric acid (GR grade) was further purified twice using a DST-1000 acid purification system (Savillex, Eden Prairie, USA).

2.3. LA-MC-ICP-MS measurement and data reduction

For *in situ* Sr isotope measurements, the combination of the high-sensitivity X skimmer cone and JET-sample cone was employed, and the mass spectrometer was operated in the low mass resolution mode. A small amount of N$_2$ (6–12 ml min^{-1}) was added to the carrier gas flow behind the signal-smoothing device by a simple Y connector. NIST SRM 610 was used to optimize the instrumental parameters, including the He and Ar gas flow rates, the torch position, the RF power setting, and the source lens settings for maximum sensitivity and optimum peak flatness. The routine data acquisition consisted of one block of 160 cycles (0.524 s integration time per cycle), with the first 50 cycles being for background collection (no laser ablation) and the remaining 110 cycles for signal collection. The detailed setup parameters of the laser system and MC-ICP-MS are listed in Table 1, including the Faraday-cup setup in the mass spectrometer.

The data reduction for LA-MC-ICP-MS analysis was conducted using Excel spreadsheets. The interference correction strategy was the same as the one reported by Tong et al. (2016). In summary, the regions of integration for both gas background and sample were selected first. Following background correction, which removes the background Kr$^+$ signals, no additional Kr peak stripping was applied. Interferences were corrected in the following sequence: (1) the interferences of ^{168}Er^{++} on ^{84}Sr, ^{170}Er^{++} and ^{170}Yb^{++} on ^{85}Rb, ^{172}Yb^{++} on ^{86}Sr, and ^{174}Yb^{++} on ^{87}Sr were corrected based on the measured signal intensities of ^{167}Er^{++}, ^{173}Yb^{++}, $^{84, 86–88}$Sr and ^{85}Rb and the natural isotope ratios of Er and Yb (Berglund and Wieser, 2011); (2) the isobaric interference of ^{87}Rb on ^{87}Sr was corrected by monitoring the ^{85}Rb signal intensity and a user-specified ^{87}Rb/^{85}Rb ratio using an exponential law for mass bias. The user-specified ^{87}Rb/^{85}Rb ratio was calculated by measuring some reference materials with a known ^{87}Sr/^{86}Sr ratio. Following the

interference corrections, mass fractionation of Sr isotopes was corrected by assuming $^{88}Sr/^{86}Sr = 8.375209$ (Jochum et al., 2009) and applying the exponential law (Russell et al., 1978).

3. Results and discussion

3.1. Ablation rate

In this study, a range of natural minerals (pyrite, garnet, albite YG0383 and Cpx HNB-8) and NIST SRM 610 glass were used to investigate the ablation rates of ns and fs laser pulses. Fig. 1 shows the relationship between the number of laser pulses and crater depth in various samples obtained by ns and fs laser ablation. When using the ns laser at a repetition rate of 10 Hz, a laser spot of 60 μm and a laser fluence of ~9.5 J cm^{-2}, the depth of ablation craters differed significantly in different types of materials (Fig. 1a). The crater depth in pyrite was significantly higher compared to silicate minerals and NIST SRM 610 glass. For albite YG0383, the lowest ablation rate of 0.026 μm per pulse was found, which was approximately 3.3 times lower than that of NIST SRM 610 (0.086 μm per pulse) (Fig. 1a). In contrast, for fs laser ablation with a repetition rate of 10 Hz, a laser spot of 60 μm and a laser fluence of ~3.8 J cm^{-2}, the ablation rates of all samples were approximately consistent (0.08–0.11 μm per pulse) (Fig. 1b). Moreover, the lower fluence of the fs laser (~3.8 J cm^{-2}) contributed the higher ablation rates for feldspar (albite YG0383), Cpx (HNB-8) and garnet, indicating the better ablation efficiency of the fs pulse relative to the ns laser for natural transparency minerals.

Although the 193 nm ultraviolet (UV) can be absorbed by most natural minerals (Günther et al., 1999), there is a fundamental difference in the ablation mechanism between ns and fs laser ablation. For the ns laser, ablation starts through the absorption of the incident laser energy by the free electrons in the target material (Liu et al., 1997; Hergenröder et al., 2006; Shaheen et al., 2012). The ablation rate of the ns laser would be influenced by the physical and chemical properties of the samples (Fig. 1a). Pyrite can effectively absorb laser energy and produce a high ablation rate during ns laser ablation (0.144 μm per pulse) because it contains many free electrons. However, free electrons normally present at low concentrations and randomly distributed in transparent minerals, such as natural silicate minerals, result in a stochastic and inefficient ablation (Liu et al., 1997; Hergenröder et al., 2006; Shaheen et al., 2012). Feldspars are transparent minerals and often lack metal elements, such as Fe. Therefore, albite YG0383 shows the lowest ablation rate (0.026 μm per pulse). For fs laser ablation, due to the high pulse intensity, the interaction of fs laser pulses with solid materials is mainly dominated by two types of non-linear absorption processes: avalanche ionization and multi-photon ionization. In multi-

photon ionization, bound electrons of the transparent material can be directly ionized by simultaneously absorbing multiple photons and forming a mass of free electrons to initiate the avalanche ionization. Then, the energy transfer of the fs pulses into the samples does not depend on already pre-existing free electrons, and the ablation event is more deterministic and initiated by a similar laser-material interaction mechanism for various materials with different physical and chemical properties (Liu et al., 1997; Shaheen et al., 2012). Therefore, the ablation rates of the fs laser are consistent for various samples, including pyrite and feldspar (Fig. 1b). This advantage not only shows the benefit of eliminating or weakening the matrix effect during the laser ablation processes but also helps to improve the analytical sensitivity for transparent minerals, such as feldspars.

3.2. Signal responses in ICP-MS

Fig. 2 shows the Sr responses (cps/μg g^{-1}) obtained from LA-ICP-MS for reference glasses (NIST SRM 610, NIST SRM 612, ATHO-G, BHVO-2G) and natural feldspars (albites YG0383 and K-feldspar Tuyk) with changing laser fluences of the ns and fs lasers. For the ns laser, Sr responses were obviously different among the NIST glasses, USGS glasses and natural feldspars (Fig. 2), which were consistent with the above studies about ablation characteristics. The Sr responses of natural feldspars obtained by the ns laser were two times lower than those of the NIST glasses at the same fluence. The lower ablation rate of feldspars was considered as the main reason. In contrast, for fs laser ablation, a similar response trend with increasing laser fluence was observed in all the samples (Fig. 2). This is in line with the expectation of the similar ablation rates for various materials ablated by the fs laser, as mentioned above. The direct and exact comparison between the ns laser and fs laser used in this study cannot be achieved due to the different energy distributions (flat peak *vs* Gaussian peak) and energy outputs. However, as a rough comparison, the Sr responses in feldspars from fs laser ablation at 3.8 J cm^{-2} were 3.4 times higher than those from the ns laser at 4.1 J cm^{-2}. In addition to higher ablation rates of the fs laser pulses, the high sensitivity observed in fs laser ablation could be related to the size of laser-generated particles. The particles produced by fs laser ablation have small sizes distributed over a narrow range (D'Abzac et al., 2012, 2013). This improves particle transport efficiency and ionization inside the ICP and consequently improves the sensitivity and signal reproducibility. However, the direct evidences between the improved signal sensitivity and the particle morphology were not provided in this study. Further investigations are needed to validate this assumption.

The promotion of signal intensity benefits the improvement of the precision for isotope ratio measurements. The within-run precisions
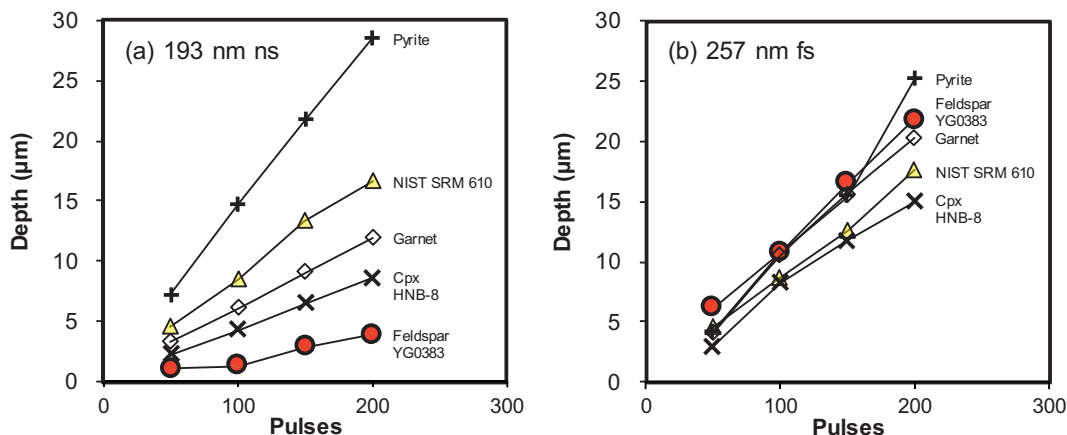

Fig. 1. Depth *vs* applied number of laser pulses for various samples using the 193 nm ns laser system with a repetition rate of 10 Hz, a laser spot of 60 μm and an energy density of ~9.5 J cm^{-2} (a) and using the 257 nm fs laser system with a repetition rate of 10 Hz, a laser spot of 60 μm and an energy density of ~3.8 J cm^{-2} (b).
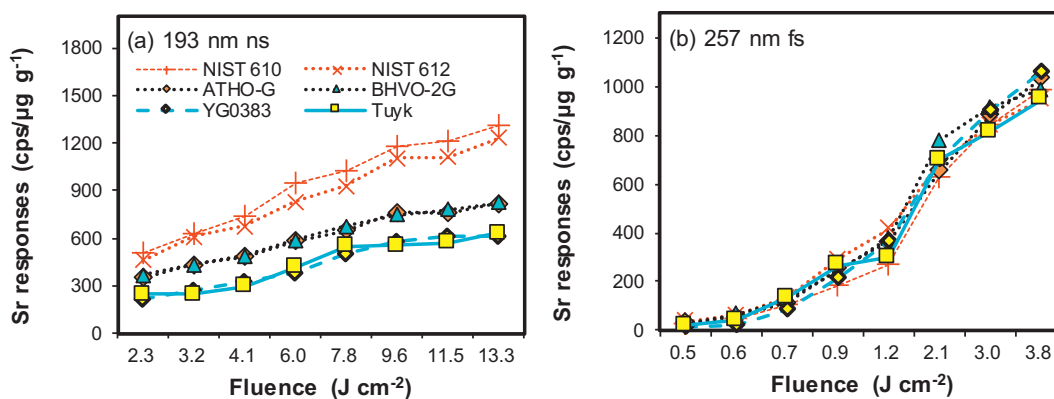
Fig. 2. The Sr signal responses (cps/µg g^{-1}) for reference glasses (NIST SRM 610, NSIT SRM 612, ATHO-G, and BHVO-2G) and nature feldspars (albites YG0383 and K-feldspar Tuyk) with changing laser fluences for the 193 nm ns laser (a) and 257 nm fs laser (b). The other laser parameters were the repetition rate of 10 Hz and the laser spot of 60 µm in both laser ablation system.

(standard error, SE, k = 2) of the $^{87}Sr/^{86}Sr$ ratio in BHVO-2G and natural albite (YG0440) by the ns and fs lasers are shown in Fig. 3. The same laser repetition rate of 10 Hz and a spot size of 60 µm were used, but the fluences were ~9.5 J cm^{-2} and 3.8 J cm^{-2} for the ns laser and fs laser, respectively. The concentrations of Sr and Rb are 396 µg g^{-1} and 9.20 µg g^{-1} for BHVO-2G and 390 µg g^{-1} and 0.23 µg g^{-1} for YG0440, respectively. The theoretical precisions, Poisson counting statistics errors (SD$_P$, Yang et al., 2011b), were calculated. As seen in Fig. 3, the observed 2SE of the $^{87}Sr/^{86}Sr$ ratio correlates well with the SD$_p$. For the fs laser, the ^{88}Sr signal intensity and 2SE of the $^{87}Sr/^{86}Sr$ ratio were approximately similar for BHVO-2G and YG0440. However, for the ns laser, the ^{88}Sr signal intensity of YG0440 was approximately 0.88 V and ~42% lower than that of BVHO-2G (1.52 V), resulting in the obvious deterioration of the 2SE of the $^{87}Sr/^{86}Sr$ ratio (Fig. 3). Obviously, the fs laser improves the analytical sensitivity and the precision for transparent minerals (feldspars) due to the better ablation efficiency. This advantage will become more apparent for the low-Sr minerals or high spatial resolution cases.

3.3. Influence of N$_2$ addition on interference correction

LA-MC-ICP-MS is a solid sample direct injection technique. Many interfering elements will be introduced into ICP-MS due to the absence of a chromatographic purification process. The main interferences of Sr isotope analysis for feldspar are Rb, Kr, calcium dimers and argides, and doubly charged Er and Yb (Ramos et al., 2004). In this section, we
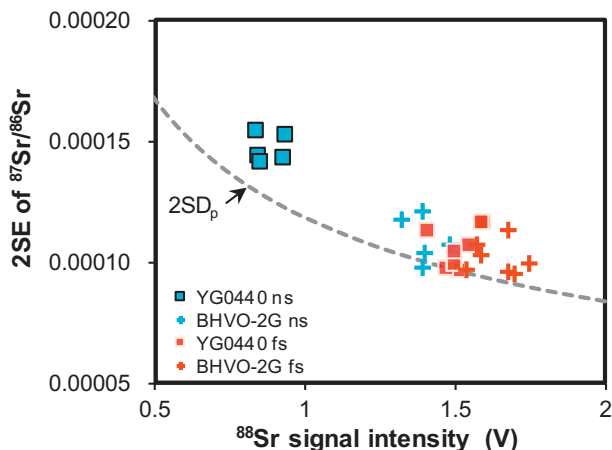

Fig. 3. Correlations between the within-run precisions (standard error, SE, k = 2) of single spot analyses and ^{88}Sr signal intensities of the reference glass BHVO-2G and natural albite (YG0440) analyzed by ns and fs laser ablation.

describe our investigation of the effect of inhibiting sensitivities of interfering elements and yields of polyatomic ions by the addition of N$_2$.

3.3.1. Calcium dimers and argides, doubly charged Er and Yb

In this study, NIST SRM 987 solutions (100 µg l^{-1}) doped with interfering elements (Er and Yb) and a Ca solution (Ca = 500 µg l^{-1}) were measured using MC-ICP-MS with a desolvation sample introduction system (Aridus II) and GE on mode. The ion beams on masses of 84, 83.5 and 86.5 were collected to represent the polyatomic ions of Calcium (CaAr$^+$/CaCa$^+$), doubly charged Er ($^{167}Er^{++}$) and Yb ($^{173}Yb^{++}$), respectively. The signal intensities of ^{88}Sr, $^{167}Er^{++}$, $^{173}Yb^{++}$ and CaAr$^+$/CaCa$^+$ as a function of N$_2$ addition are illustrated in Fig. 4. Increasing N$_2$ from 0 ml min^{-1} to 12 ml min^{-1} leads to a gradual decrease in the signal intensity of ^{88}Sr. Sr with a low ionization potential (IP = 5.7 eV) can be completely ionized in a typical ICP; therefore, its sensitivity cannot be improved by increasing the temperature of ICP by adding N$_2$. $^{167}Er^{++}$ and $^{173}Yb^{++}$ were suppressed at a similar extent of Sr (Fig. 4b and c, respectively). However, the signal intensity of CaAr$^+$/CaCa$^+$ shows a significant decrease associated with an increase in the N$_2$ flow rate, such as the signal suppression of 6.5 times and 11.7 times for N$_2$ additions of 6 ml min^{-1} and 12 ml min^{-1}, respectively. This may be due to the higher ICP temperature by adding N$_2$, which could result in decomposition of the polyatomic ion.

3.3.2. Krypton (Kr)

The noble gas krypton (Kr) interferes with masses ^{84}Sr and ^{86}Sr and is therefore an important interference that needs to be corrected. The source of the Kr is the argon (and helium) gas used to transport the sample into the plasma. The amount of krypton in the argon (and helium) gas is supplier dependent. Woodhead et al. (2005) observed that the Kr abundances in the Ar supply vary largely between different batches, with a total Kr contribution of approximately 20 mV. Ramos et al. (2004) reported that Kr is present in low levels as an impurity in the argon gas (typically < 1 mV for ^{83}Kr) and in the helium transfer gas used during laser ablation (< 3 mV for ^{83}Kr). Kimura et al. (2013) suggested that both signal suppression and enhancement are possible on Kr baselines due to (1) the suppression by laser aerosol loading and (2) the enhancement from Kr in the ablated samples.

In this section, the natural albite (YG0383) was analyzed by fs-LA-MC-ICP-MS in GE on mode. Fig. 5 presents the average signal intensities of $^{88}Sr^+$ from YG0383 and $^{83}Kr^+$ in the background without laser firing as a function of N$_2$ addition. With the addition of N$_2$ from 0 ml min^{-1} to 6 ml min^{-1} and 12 ml min^{-1}, the signal intensities of $^{88}Sr^+$ in YG0383 decreased from 3.3 V to ~2.5 V (1.32 times) and ~1.9 V (1.73 times), respectively (Fig. 5a). However, the signal intensities of $^{83}Kr^+$ decreased significantly from 0.00163 V to 0.00027 V (6.0 times) and 0.00013 V (12.5 times), respectively (Fig. 5b). Kr has a high first
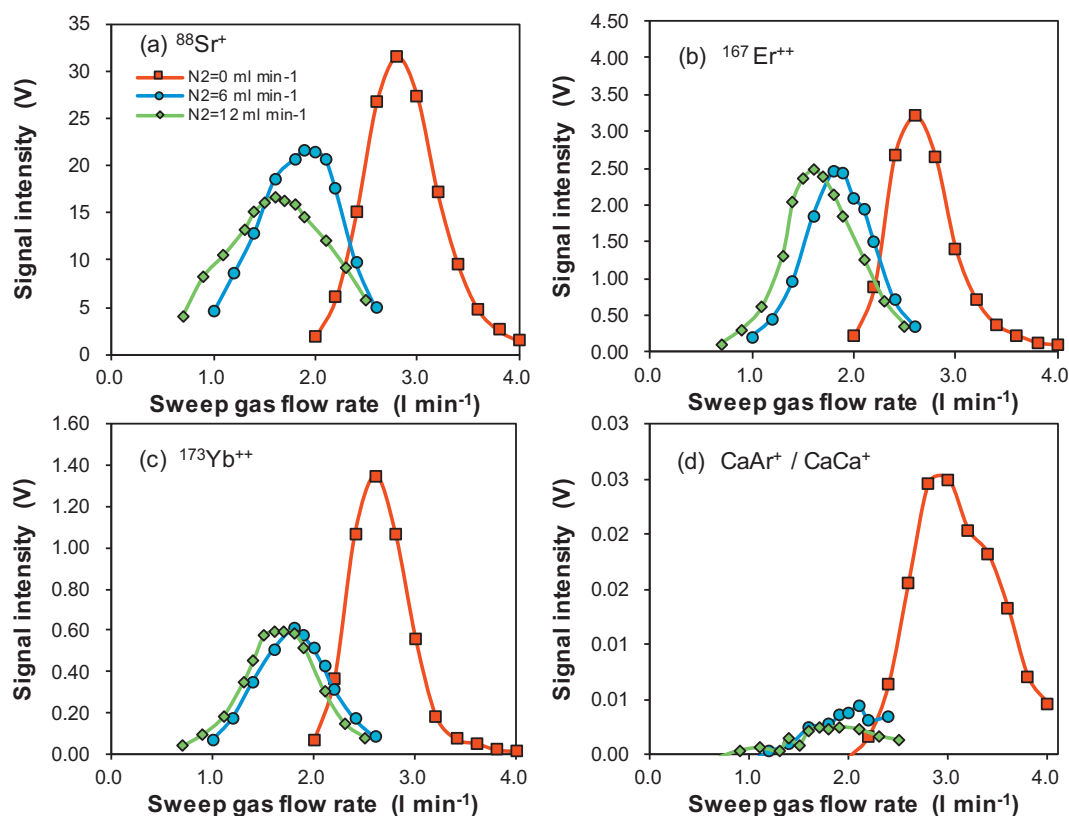
Fig. 4. The integrated average signal intensities of $^{88}Sr^+$, $^{167}Er^{++}$, $^{173}Yb^{++}$ and $CaAr^+/CaCa^+$ from a series of NIST SRM 987 solutions as a function of sweep gas flow rate combined in both normal and N_2 (N_2 = 6–12 ml min^{-1}) modes.

ionization energy (14.0 eV) relative to Sr (4.2 eV), which could theoretically be improved the sensitivity due to the increase in ICP temperature by adding N_2. However, the reverse experimental results in Fig. 5 indicated that another important parameter must be considered. The evaporation enthalpies of Kr and Sr are 9.0 kJ mol^{-1} and 144 kJ mol^{-1}, respectively. With the increase in ICP temperature by adding N_2, Kr could evaporate and ionize earlier than Sr near the torch, resulting in a separation of the optimum-ICP parameters between Kr and Sr. Then, the shorter sampling depth (the Z-axis value) and the higher sample gas flow rate should increase the sensitivity of Kr. Fig. 5b shows that the signal intensities of Kr increase gradually with the sample gas flow rate from 0.10 ml min^{-1} to 0.58 ml min^{-1}, which is consistent with our speculation. To the best of our knowledge, this study shows for the first time that the addition of nitrogen dramatically suppressed the Kr interference, which would significantly benefit for

the in situ Sr isotopic analysis by LA-MC-ICP-MS. Further investigations are needed to reveal the exact mechanism behind this phenomenon.

3.3.3. Rubidium (Rb)

Rubidium (Rb) is a well-known interference with ^{87}Sr for the $^{87}Sr/^{86}Sr$ ratio analysis. Feldspar samples often contain a large amount of Rb, which can substitute for K in the way of isomorphism. The isobaric interference of ^{87}Rb with ^{87}Sr was corrected by the measured $^{86}Sr/^{88}Sr$ ratio and a natural $^{87}Rb/^{85}Rb$ ratio of 0.38571 (Ramos et al., 2004). In this method, the mass bias of Rb is assumed to be consistent with that of Sr. However, it has been recognized in recent years that different elements can isotopically fractionate differently in MC-ICP-MS, such as Pb and Tl (Zhang et al., 2016). An alternative approach is using a certified reference material to calibrate a user-specified $^{87}Rb/^{85}Rb$ ratio (Jackson and Hart, 2006; Jochum et al., 2009; Tong
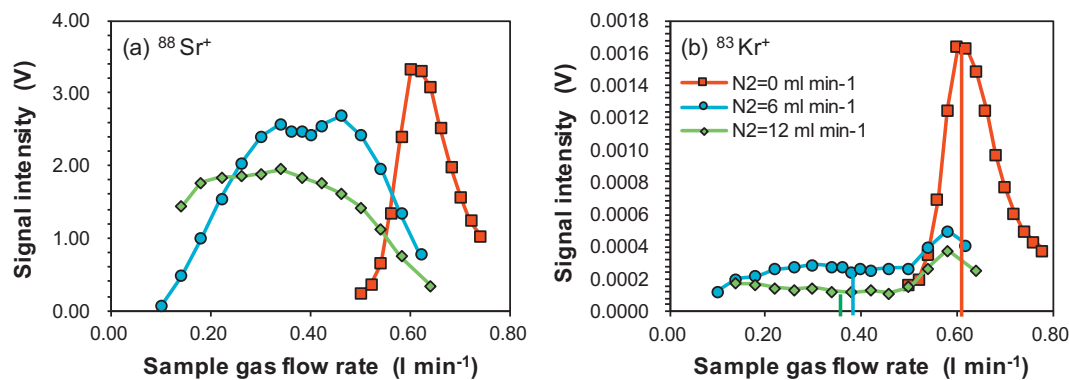

Fig. 5. Fig. 5 (a) The average signal intensities of $^{88}Sr^+$ obtained from YG0383 by fs-laser ablation MC-ICP-MS as a function of N_2 addition (0, 6, 12 ml min^{-1}). (b) The average signal intensities of $^{83}Kr^+$ in the gas background without laser firing as a function of N_2 addition (0, 6, 12 ml min^{-1}). The vertical lines in (b) represent the optimum range of sample gas flow rate for $^{88}Sr^+$ signal intensity at different N_2 gas flow rates.

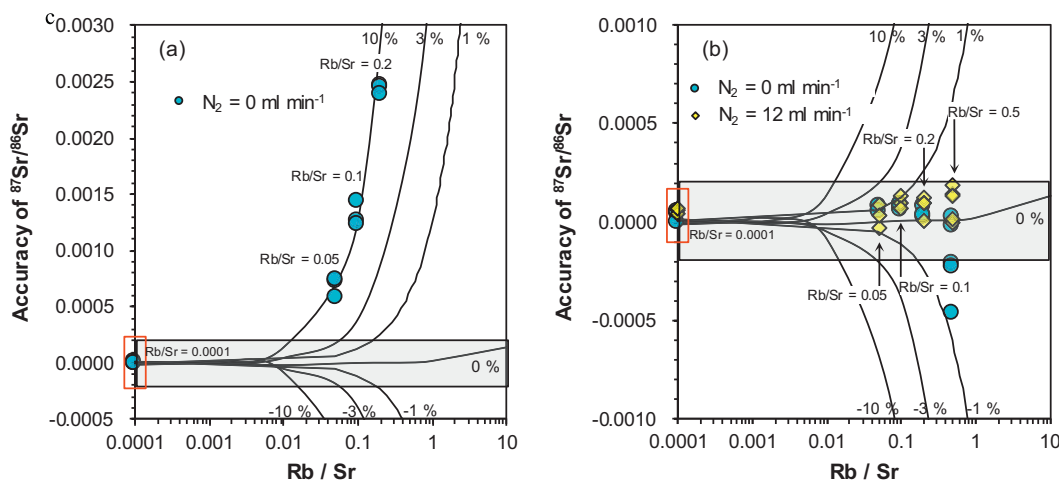**Fig. 6.** (a) The accuracy of $^{87}Sr/^{86}Sr$ for a series of NIST SRM 987 doped with increasing amounts of Rb at normal and N_2 (N_2 = 12 ml min^{-1}) modes. The interference of ^{87}Rb on ^{87}Sr was corrected by the natural isotopic composition of Rb and f_{Sr}. (b) The same data was corrected using a user-specified f_{Rb}, which was obtained from a NIST SRM 984 solution (100 µg l^{-1}). Gray fields represent the accuracy of $^{87}Sr/^{86}Sr$ < 0.0002. The black lines in each panel are simulated lines with different Δf_{Rb} values.

et al., 2016). The essence of the latter approach is the use of two different mass bias factors (f) for Sr and Rb. Through determining more accurate Rb mass bias factors (f_{Rb}), we were able to measure high Rb/Sr ratio materials.

In this section, we first simulated the effect of Δf_{Rb} at different Rb/Sr ratio conditions, as shown in Fig. 6. Δf_{Rb} is the deviation between the used f_{Rb} and the true f_{Rb}. As seen in Fig. 6a, the black lines represent the accuracies of the $^{87}Sr/^{86}Sr$ ratios calibrated by different Δf_{Rb} values from − 10% to 10%. If Δf_{Rb} values are > 10% or − 10%, the accuracies of the $^{87}Sr/^{86}Sr$ ratios will be > 0.0002 for the samples with Rb/Sr ratios > ~0.01, while the superior accuracies of < 0.0002 can be obtained for the samples with higher Rb/Sr ratios > 0.10 if the Δf_{Rb} values are smaller than 1%. In other words, the higher Rb/Sr ratio samples can be measured accurately when the used f_{Rb} is closer to the true f_{Rb}.

After the mathematical simulation, we have undertaken a series of tests using Rb-doped (NIST SRM 984 Rb solution) NIST SRM 987 solutions (Fig. 6). In Fig. 6a, the mass bias factor of Sr (f_{Sr}) was used to correct the mass bias of Rb. In the normal condition (N_2 = 0 ml min^{-1}), the deviation of f_{Rb} and f_{Sr} (Δf_{Rb}) was up to ~10%, resulting in the deviation of the $^{87}Sr/^{86}Sr$ ratios of > 0.0002 for Rb/Sr ratios > 0.05. The measured results were well overlapped with the simulated lines. In Fig. 6b, the same data in Fig. 6a were processed again using a user-specified f_{Rb}, which was obtained from a Rb standard solution (NIST SRM 984, 100 µg l^{-1}). The results show that the accuracy of the $^{87}Sr/^{86}Sr$ ratios significantly improved to < 0.0002, even with Rb/Sr ratio = 0.2. Conclusively, the accuracy of f_{Rb} and the Rb/Sr ratio are important parameters for the exact Rb-interference correction.

An interesting finding was that the sensitivities of Rb in the normal condition (N_2 = 0 ml min^{-1}) were always higher than those of Sr. The measured Rb/Sr signal ratios were thus higher than the reference Rb/Sr ratios in the samples (Fig. 7). With the addition of N_2 (12 ml min^{-1}), the sensitivities of Rb and Sr suffered an obvious suppression. However, Rb was worse, reducing the Rb/Sr signal ratios by approximately 1.47 times (Fig. 7). The first ionization energy of Rb (5.7 eV) is similar to that of Sr (4.2 eV), but the evaporation enthalpy of Rb (72.2 kJ mol^{-1}) is 2 times lower than that of Sr (144 kJ mol^{-1}). Therefore, the difference of evaporation enthalpies could be the main reason for the different degrees of signal suppression of Rb and Sr with the addition of N_2. The advantage of reducing the Rb/Sr signal ratio with the addition of N_2 is the more accurate correction of Rb interference for the rich-Rb samples. This is demonstrated in Fig. 6b; with the addition of N_2 (12 ml min^{-1}), the accuracies of the $^{87}Sr/^{86}Sr$ ratios were better than 0.0002 even with Rb/Sr ratio = 0.5.
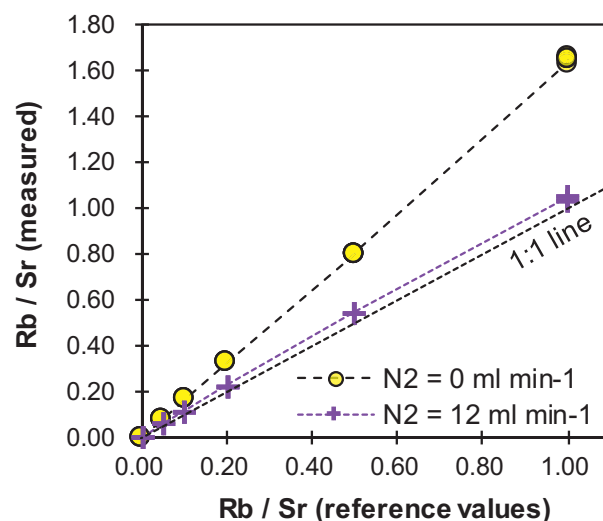

Fig. 7. Effect of N_2 addition on Rb/Sr signal ratios evaluated by solution-MC-ICP-MS. The data was obtained by analyzed a series of NIST SRM 987 doped with increasing amounts of Rb at normal and N_2 (N_2 = 12 ml min^{-1}) modes.

3.3.4. The effect of adding N_2 for Sr isotope analysis

Three feldspars (YG0383, YG0440, Tuyk) were analyzed by fs-LA-MC-ICP-MS to evaluate the effect of interference suppression by adding N_2. Fig. 8 presents the accuracies of the $^{87}Sr/^{86}Sr$ ratios and the $^{84}Sr/^{86}Sr$ ratios as a function of N_2. With the addition of N_2, both stability and accuracy of the measured $^{87}Sr/^{86}Sr$ ratios improved, especially for Tuyk, which is Rb-rich K-feldspar and has a high Rb/Sr ratio (0.46) (Fig. 8a). More significant improvements occurred in the $^{84}Sr/^{86}Sr$ ratios. In the normal condition (N_2 = 0 ml min^{-1}), residual analytical biases of $^{84}Sr/^{86}Sr$ in three feldspars were observed after on-peak background subtractions and mass-fractionation corrections (Fig. 8b). With the addition of N_2, the accuracies of the $^{84}Sr/^{86}Sr$ ratios improved, indicating that either Ca polyatomic interferences or Kr effects (such as Kr baseline suppression or release of trace Kr from the sample) have been inhibited efficiently. Though the addition of N_2 reduces the sensitivity of Sr in both solution and LA modes, higher suppression of Kr, Rb and polyatomic interferences improves the signal-to-noise ratio and thus increases the accuracy and precision of Sr isotope analysis.
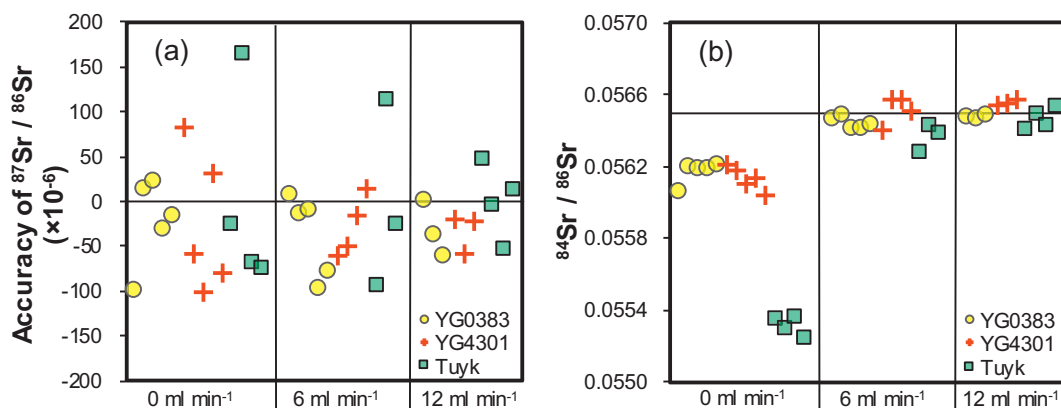
Fig. 8. Effect of N_2 addition on the $^{87}Sr/^{86}Sr$ ratios (a) and $^{84}Sr/^{86}Sr$ ratios (b) for three natural feldspars (YG0383, YG0440, Tuyk). The horizontal black line in Fig. 8(b) represents the natural ratio of $^{84}Sr/^{86}Sr$ (0.05657).

4. Application to natural samples

According to the investigation of ablation characteristics of the fs laser and the effects of the addition of N_2, an improved *in situ* Sr isotopes analytical method was established. The feasibility and flexibility of the proposed method were verified by analyzing various natural samples.

4.1. Feldspar crystals

Four natural feldspars were analyzed, and the results are shown in Table 2 and Fig. 9. The first three feldspars are plagioclases with different An values (CaO / (2 × Na_2O + 2 × K_2O + CaO) in mol.%) and Sr concentrations. The concentrations of Rb in the three feldspars are very low (< 0.67 μg g^{-1}). The measured results of the $^{87}Sr/^{86}Sr$ ratios for the three feldspars using fs-LA-MC-ICP-MS with N_2 = 12 ml min^{-1} were 0.713724 ± 0.000030 (YG0440: 0.713718 using TIMS), 0.710909 ± 0.000040 (YG0383: 0.710919 using TIMS) and 0.703421 ± 0.000030 (YG4301: 0.703426 using TIMS). The accuracies of the averaged values were from − 0.000014 to 0.000009. The measurement reproducibility, defined as two times of the relative standard deviation (RSD, k = 2) of repeated analyses, was better than 0.000042. In addition, the $^{84}Sr/^{86}Sr$ ratios were relatively constant among the three feldspars and similar to the natural ratio of 0.05657 (Tong et al., 2016). These data confirmed the availability of the proposed method for the common and low Rb/Sr ratio plagioclase samples.

The fourth feldspar sample in Table 2 is a K-feldspar phenocryst (Tuyk), which has been used as an in-house reference material for *in situ* Pb isotope analysis (Zhang et al., 2015). The concentrations of Rb and Sr in the Tuyk are 285 μg g^{-1} and 620 μg g^{-1}, respectively. The Rb/Sr ratio is approximately 0.46, which is higher than the critical value of 0.2 defined by Davidson et al. (2001) and Jackson and Hart (2006). In addition to using fs-laser ablation and N_2, we selected three reference glasses with high Rb/Sr ratios, StHs6/80-G (Rb/Sr ratio = 0.06), T1-G (Rb/Sr ratio = 0.28) and GSE-1G (Rb/Sr ratio = 0.80), to calculate the user-specified f_{Rb} for correcting Rb interference. The average value for $^{87}Sr/^{86}Sr$ acquired by fs-LA-MC-ICP-MS was 0.710325 ± 0.000297

(SD, k = 2), which was significantly higher than the TIMS value (0.710206). The analytical accuracy and reproducibility (RSD, k = 2) were 0.000167 and 0.000417, respectively. Obviously, for samples with high Rb/Sr ratios, the interference of Rb seriously inhibited the accuracy and precision of $^{87}Sr/^{86}Sr$ ratio analysis. However, our method presents a significant improvement in the accuracy and reproducibility for high Rb/Sr feldspar samples relative to previous studies. For example, Davidson et al. (2001) reported accuracy and reproducibility were 0.0059 and 0.0011, respectively, for plagioclases with a high Rb/Sr ratio (0.52). Jackson and Hart (2006) reported that the basalt glass samples with high Rb/Sr ratios (0.14) had large errors (0.000505).

The above results also demonstrated that the four feldspars, which have various concentrations of the major elements, Sr and Rb, had homogeneous Sr isotope compositions and thus are suitable as reference materials for *in situ* Sr isotope analysis, including feldspar samples with high Rb/Sr ratios (< 0.5).

Our research interest is to decipher the origin of mafic microgranular enclaves (MMEs) in granitoids. In past decades, several models have been proposed to explain the petrogenesis of these MMEs, including residues after partial melting, xenoliths of the country rocks, cumulates formed by early crystallization, or mafic magma enclaves generated during magma mixing (Davidson et al., 2007). Commonly, MMEs contain lots of plagioclases, which are sensitive to the geochemical variations of the magma chamber. Therefore, tracing the $^{87}Sr/^{86}Sr$ ratios that vary from core to rim of those plagioclases can provide unique information for understanding the petrogenesis of the MMEs. However, plagioclases in MMEs usually have small grain sizes (200–300 μm) with wide ranges of Rb/Sr ratios. Thus, it is a great challenge for high-precision Sr isotope measurements. To verify our experimental method, we chose MMEs from the Ganze-Daocheng granitic belt in the Yidun arc terrane as a case to study (Wu et al., 2016). Based on careful petrographic observation, two plagioclase grains from thin sections were analyzed by fs-LA-MC-ICP-MS. The analytical results are listed in Fig. 9. As shown in Fig. 9, each plagioclase has a diameter of approximately 200–400 μm. The line scan mode was used with spot size of 45 μm, repetition rate of 30 Hz and line scanning speed of 5 μm s^{-1}. Both plagioclases have distinct $^{87}Sr/^{86}Sr$

Table 2
Sr isotope ratios for four natural feldspars measured by TIMS and fs-LA-MC-ICP-MS.

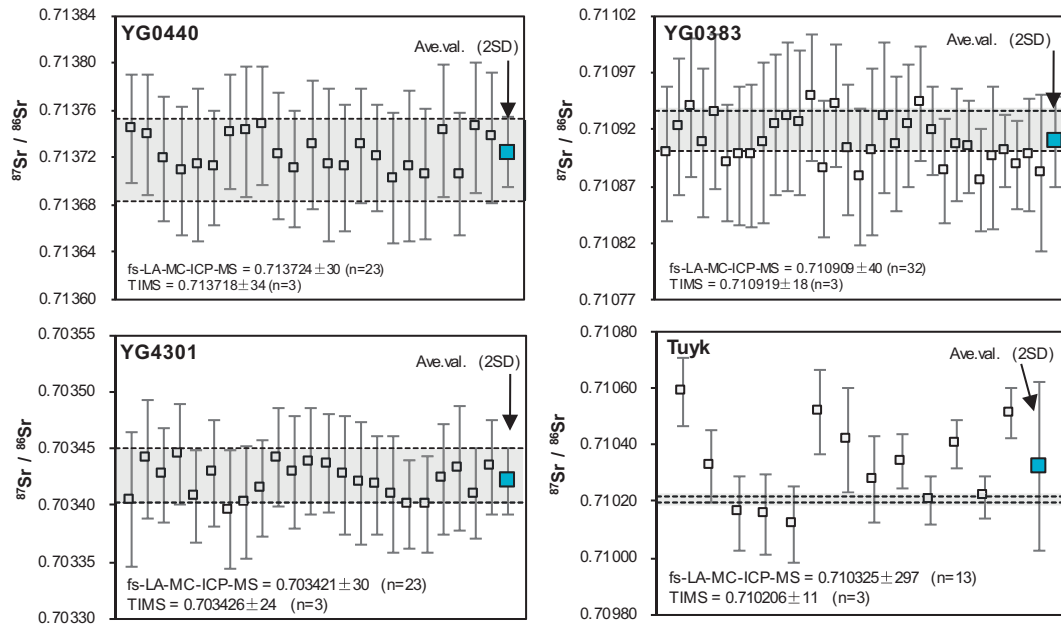|	TIMS (n = 3)	fs-LA-MC-ICP-MS					An%	Sr	Rb	Rb/Sr
	87Sr/86Sr	87Sr/86Sr	2SD	84Sr/86Sr	2SD	n		μg g^{-1}		
YG0440	0.713718 ± 34	0.713724	0.000030	0.05636	0.00017	23	9	390	0.23	0.0006
YG0383	0.710919 ± 18	0.710909	0.000040	0.05646	0.00020	32	10	1511	0.00	0.0000
YG4301	0.703426 ± 24	0.703421	0.000030	0.05642	0.00024	23	51	1058	0.67	0.0006
Tuyk	0.710206 ± 11	0.710325	0.000297	0.05641	0.00015	13	0	620	285	0.46

Fig. 9. Sr isotope ratios for four natural feldspars measured by TIMS and fs-LA-MC-ICP-MS. The error bars represent ± 2 standard errors (SE). The gray shadows represent the reference range obtained by TIMS. Ave. val., average value; TIMS, values determined by TIMS.

ratios from core to rim (Fig. 10), which could indicate that the Sr isotopes of the initial plagioclase grain does not in equilibrium with surround melt. Therefore, the variation of Sr isotopes in the same plagioclase grain may record the magma mixing process. Further studies and evidences are required to confirm this assumption. Nevertheless, it demonstrated that the fs-LA-ICP-MS analysis method established in this study can trace the variation of Sr isotopic compositions even in one small feldspar grain and provide a new perspective for exploring magma origin and evolution.

4.2. Clinopyroxene with low Sr concentration

Clinopyroxene (Cpx) is one of the major hosts of Sr in the lithospheric mantle along with plagioclase, and its Sr isotopic composition has been widely used to provide information on metasomatic agents affecting the lithospheric mantle (Schmidberger et al., 2003; Tong et al., 2016). The low content of Sr in Cpx is an important constraint on precise isotopic determination of Sr by LA-MC-ICP-MS. In our fs-based system, the use of high repetition rates (up to 1 kHz) combined with higher energy provides higher ion currents accompanied by improved

precision and accuracy. A natural Cpx megacryst (HNB-8, $Sr = 89.2 \, \mu g \, g^{-1}$) which has been analyzed for Sr isotope ratios using TIMS and ns-LA-MC-ICP-MS by Tong et al. (2016), was selected in this study. Fig. 11 shows the variation of the $^{87}Sr/^{86}Sr$ ratios in HNB-8 as a function of laser frequency and laser fluence. The line scanning mode for a 60 μm spot size was used. The measured $^{87}Sr/^{86}Sr$ ratios obtained at low ablation frequencies (20 Hz and 50 Hz) and a low ablation fluence ($1.17 \, J \, cm^{-2}$) were quite scattered due to the low Sr signal intensity. In contrast, at high frequencies (> 100 Hz) and high fluences ($> 2.06 \, J \, cm^{-2}$), the measured $^{87}Sr/^{86}Sr$ ratios in HNB-8 were consistent and agree with the value of TIMS within uncertainty. Compared to previous research, the reproducibility of the $^{87}Sr/^{86}Sr$ ratios of HNB-8 in this study was 0.0001 (2SD) and 3 times lower than that of ns laser ablation (0.0003, 2SD) (Tong et al., 2016). However, using the line scan mode in this study produced a $60 \times 400 \, \mu m$ laser trough with an area of $24,000 \, \mu m^2$, which was 2.1 times larger than that produced by ns laser ablation (spot size of 120 μm, 11,304 μm²). Although this comparison is not exact, we can understand that the fs laser has a strong flexibility to address different types of samples.)
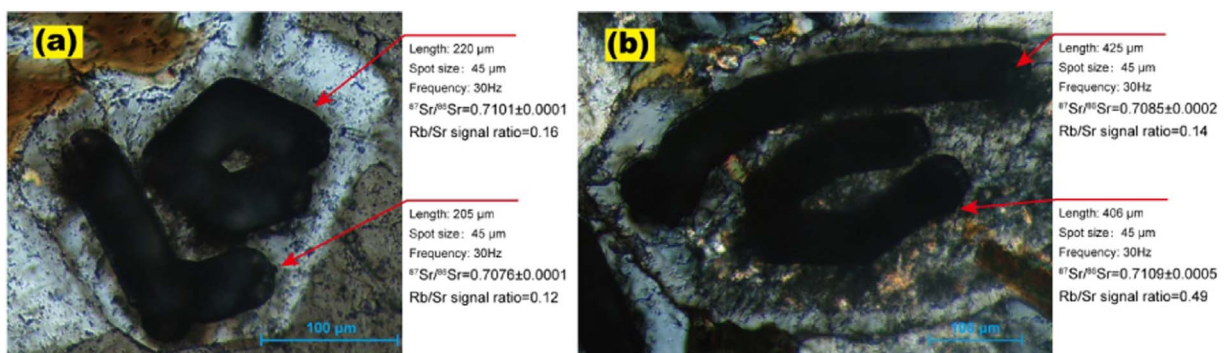

Fig. 10. $^{87}Sr/^{86}Sr$ ratios of two plagioclases from MMEs determined using fs-LA-MC-ICP-MS combined with the addition of N_2 (12 ml min^{-1}). The line scanning mode was used. The detailed laser parameters are listed in each panel. The back linear regions in each panel are laser ablated troughs.
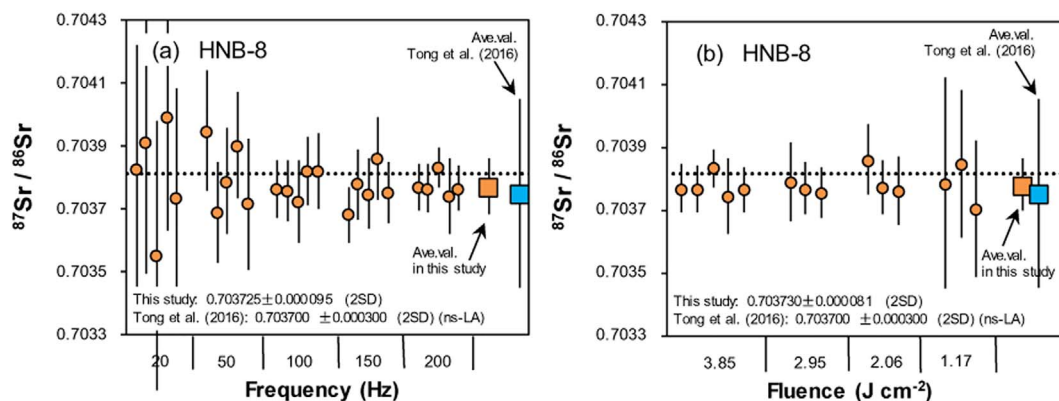
Fig. 11. $^{87}Sr/^{86}Sr$ ratios of Cpx crystal HNB-8 determined by fs-LA-MC-ICP-MS as a function of laser frequency (a) and laser fluence (b). The data for the $^{87}Sr/^{86}Sr$ ratios from low frequency and low fluence were not collected to calibrate the average value. The error bars represent ± 2 standard errors (2SE). The black dotted lines represent the solution values (Tong et al., 2016). The data of ns laser ablation for HNB-8 published by Tong et al. (2016) was plotted.

5. Conclusion

In this study, we first compared the differences in ablation characteristics, signal responses and precisions of Sr isotope ratio analyses between ns LA and fs LA. The results indicated that the advantages of fs LA were not only the higher ablation rates relative to ns LA but also the elimination of matrix-dependent ablation behavior, producing consistent ablation rates and signal responses in a variety of materials. The natural transparent minerals that are difficult to ablate by ns laser pulses, such as feldspars, gain the maximum benefit from fs LA. As a rough comparison, the Sr responses in feldspars from fs laser ablation at 3.8 J cm^{-2} were 3.4 times higher than those from the ns laser at 4.1 J cm^{-2}, resulting in a significant improvement of the precision of Sr isotope analysis, especially for the low-Sr minerals or high spatial resolution cases.

We demonstrated that sensitivities of Sr, Rb and Kr and yields of polyatomic interferences ($CaAr^+/CaCa^+$) and doubly charged Er ($^{167}Er^{++}$) and Yb ($^{173}Yb^{++}$) were simultaneously suppressed by the addition of N_2. However, the effect of suppression on Sr was obviously lower than that on Rb, Kr and polyatomic interferences ($CaAr^+/CaCa^+$), resulting in the enhancement of the signal-to-noise ratio. This improved the accuracy of the $^{84}Sr/^{86}Sr$ ratios, which are easily interfered with by Ca polyatomic interferences and Kr and the by external precision of the $^{87}Sr/^{86}Sr$ ratio analysis. In addition, due to the decrease in the Rb/Sr signal ratio, the samples with a Rb/Sr ratio < 0.5 can be measured within the accuracy of $^{87}Sr/^{86}Sr$ < 0.0002 using a user-specified f_{Rb}.

Combining the high ablation efficiency of the fs laser with the capacity of suppressing the interference factors by adding N_2, the improved *in situ* Sr isotopic analysis method using a 257 nm fs laser was established and employed to analyze four natural feldspars, including K-feldspars with high Rb/Sr ratios (0.46). The good accuracy and external reproducibility of $^{87}Sr/^{86}Sr$ for the four feldspars not only confirmed the availability of the proposed method but also suggested that the four natural feldspars have homogeneous Sr isotope compositions and are suitable candidates for matrix-matched feldspar reference materials.

Despite the somewhat lower accuracy and precision of laser ablation analyses of Sr isotopes compared with the conventional solution measurements, especially for the small samples with low-Sr concentration or high Rb/Sr ratios, LA-MC-ICP-MS can provide useful information on small-scale Sr isotopic variations in many geological applications. In this study, two plagioclases in mafic microgranular enclaves (MMEs) with small grain sizes (200–300 μm) and wide ranges of Rb/Sr ratios were analyzed and showed obvious variations of the $^{87}Sr/^{86}Sr$ ratios from core to rim. In addition, the high frequency of the fs laser was used to analyze the natural Cpx megacryst with a low-Sr concentration

(HNB-8, Sr = 89.2 μg g^{-1}). The analytical reproducibility of the $^{87}Sr/^{86}Sr$ ratios in HNB-8 analyzed by the fs laser was 3 times lower than that of the ns laser. Both cases showed the feasibility and flexibility of the fs-LA-MC-ICP-MS analysis method established in this study.

Appendix A. Supplementary data

Supplementary data to this article can be found online at https://doi.org/10.1016/j.chemgeo.2017.12.018.

References

Balter, V., Telouk, P., Reynard, B., Braga, J., Thackeray, F., Albarède, F., 2008. Analysis of coupled Sr/Ca and 87Sr/86Sr variations in enamel using laser-ablation tandem quadrupole-multicollector ICPMS. Geochim. Cosmochim. Acta 72 (16), 3980–3990.

Barnettjohnson, R., Ramos, F.C., Grimes, C.B., Macfarlane, R.B., 2005. Validation of Sr isotopes in otoliths by laser ablation multicollector inductively coupled plasma mass spectrometry (LA-MC-ICPMS): opening avenues in fisheries science applications. Can. J. Fish. Aquat. Sci. 62 (11), 2425–2430.

Berglund, M., Wieser, M.E., 2011. Isotopic Compositions of the Elements 2009 (IUPAC Technical Report). pp. 1102–1103.

Bian, Q., Garcia, C.C., Koch, J., Niemax, K., 2006. Non-matrix matched calibration of major and minor concentrations of Zn and Cu in brass, aluminium and silicate glass using NIR femtosecond laser ablation inductively coupled plasma mass spectrometry. J. Anal. At. Spectrom. 21 (2), 187–191.

Bizzarro, M., Simonetti, A., Stevenson, R.K., Kurszlaukis, S., 2003. In situ 87Sr/86Sr investigation of igneous apatites and carbonates using laser-ablation MC-ICP-MS. Geochim. Cosmochim. Acta 67 (2), 289–302.

Borisova, A.Y., Freydier, R., Polvé, M., Salvi, S., Candaudap, F., Aigouy, T., 2008. In situ multi-element analysis of the Mount Pinatubo quartz-hosted melt inclusions by NIR femtosecond laser ablation-inductively coupled plasma-mass spectrometry. Geostand. Geoanal. Res. 32 (2), 209–229.

Campos-Alvarez, N.O., Samson, I.M., Fryer, B.J., Ames, D.E., 2010. Fluid sources and hydrothermal architecture of the Sudbury structure: constraints from femtosecond LA-MC-ICP-MS Sr isotopic analysis of hydrothermal epidote and calcite. Chem. Geol. 278 (3), 131–150.

Charlier, B.L.A., Ginibre, C., Morgan, D., Nowell, G.M., Pearson, D.G., Davidson, J.P., Ottley, C.J., 2006. Methods for the microsampling and high-precision analysis of strontium and rubidium isotopes at single crystal scale for petrological and geochronological applications. Chem. Geol. 232 (3–4), 114–133.

Chen, K.Y., Yuan, H.L., Bao, Z.A., Zong, C., Dai, M.N., 2014. Precise and accurate in situ

determination of lead isotope ratios in NIST, USGS, MPI-DING and CGSG glass reference materials using femtosecond laser ablation MC-ICP-MS. Geostand. Geoanal. Res. 38 (1), 5–21.

Chen, W.T., Zhou, M.F., Gao, J.F., Zhao, T.P., 2015. Oscillatory Sr isotopic signature in plagioclase megacrysts from the Damiao anorthosite complex, North China: implication for petrogenesis of massif-type anorthosite. Chem. Geol. 393–394, 1–15.

Chmeleff, J., Horn, I., Steinhoefel, G., von Blanckenburg, F., 2008. In situ determination of precise stable Si isotope ratios by UV-femtosecond laser ablation high-resolution multi-collector ICP-MS. Chem. Geol. 249 (1–2), 155–166.

Christensen, J.N., Halliday, A.N., Lee, D.C., Hall, C.M., 1995. In situ Sr isotopic analysis by laser ablation. Earth Planet. Sci. Lett. 136 (1–2), 79–85.

Copeland, S.R., Sponheimer, M., Lee-Thorp, J.A., Roux, P.J.L., Ruiter, D.J.D., Richards, M.P., 2010. Strontium isotope ratios in fossil teeth from South Africa: assessing laser ablation MC-ICP-MS analysis and the extent of diagenesis. J. Anal. At. Spectrom. 37 (7), 1437–1446.

D'Abzac, F., Seydoux-Guillaume, A., Chmeleff, J., Datas, L., Poitrasson, F., 2012. In situ characterization of infrared femtosecond laser ablation in geological samples. Part B: the laser induced particles. J. Anal. At. Spectrom. Vol. 27, 108–119.

D'Abzac, F., Beard, B.L., Czaja, A.D., Konishi, H., Schauer, J.J., Johnson, C.M., 2013. Iron isotope composition of particles produced by UV-femtosecond laser ablation of natural oxides, sulfides, and carbonates. Anal. Chem. 85, 11885–11892.

Davidson, J., Tepley Iii, F., Palacz, Z., Meffan-Main, S., 2001. Magma recharge, contamination and residence times revealed by in situ laser ablation isotopic analysis of feldspar in volcanic rocks. Earth Planet. Sci. Lett. 184 (2), 427–442.

Davidson, J.P., Morgan, D.J., Charlier, B.L.A., Harlou, R., Hora, J.M., 2007. Microsampling and isotopic analysis of igneous rocks: implications for the study of magmatic systems. Annu. Rev. Earth Pl. Sci. 35 (1), 273–311.

Durrant, S.F., 1994. Feasibility of improvement in analytical performance in laser ablation inductively coupled plasma-mass spectrometry (LA-ICP-MS) by addition of nitrogen to the argon plasma. Fresenius J. Anal. Chem. 349 (10 – 11), 768–771.

Fernández, B., Claverie, F., Pécheyran, C., Donard, O.F.X., Claverie, F., 2007. Direct analysis of solid samples by fs-LA-ICP-MS. TrAC-trend. Anal. Chem. 26 (10), 951–966.

Fliegel, D., Frei, C., Fontaine, G.H., Hu, Z.C., Gao, S., Gunther, D., 2011. Sensitivity improvement in laser ablation inductively coupled plasma mass spectrometry achieved using a methane/argon and methanol/water/argon mixed gas plasma. Analyst 136 (23), 4925–4934.

Freydier, R., Candaudap, F., Poitrasson, F., Arbouet, A., Chatel, B., Dupre, B., 2008. Evaluation of infrared femtosecond laser ablation for the analysis of geomaterials by ICP-MS. J. Anal. At. Spectrom. 23 (5), 702–710.

Fu, J.L., Hu, Z.C., Zhang, W., Yang, L., Liu, Y.S., Li, M., Zong, K.Q., Gao, S., Hu, S.H., 2016. In situ sulfur isotopes (δ34S and δ33S) analyses in sulfides and elemental sulfur using high sensitivity cones combined with the addition of nitrogen by laser ablation MC-ICP-MS. Anal. Chim. Acta 911, 14–26.

Gagnevin, D., Daly, J.S., Poli, G., Morgan, D., 2005. Microchemical and Sr isotopic investigation of zoned K-feldspar megacrysts: insights into the petrogenesis of a granitic system and disequilibrium crystal growth. J. Petrol. 46 (8), 1689–1724.

Galler, P., Limbeck, A., Boulyga, S.F., Stingeder, G., Hirata, T., Prohaska, T., 2007. Development of an on-line flow injection Sr/matrix separation method for accurate, high-throughput determination of Sr isotope ratios by multiple collector-inductively coupled plasma-mass spectrometry. Anal. Chem. 79 (13), 5023–5029.

Guillong, M., Heinrich, C.A., 2007. Sensitivity enhancement in laser ablation ICP-MS using small amounts of hydrogen in the carrier gas. J. Anal. At. Spectrom. 22 (12), 1488–1494.

Günther, D., Jackson, S.E., Longerich, H.P., 1999. Laser ablation and arc/spark solid sample introduction into inductively coupled plasma mass spectrometers. Spectrochim. Acta B At. Spectrosc. 54 (3), 381–409.

He, D.T., Liu, Y.S., Tong, X.R., Zong, K.Q., Hu, Z.C., Gao, S., 2013. Multiple exsolutions in a rare clinopyroxene megacryst from the Hannuoba basalt, North China: implications for subducted slab-related crustal thickening and recycling. Lithos 177 (3), 136–147.

Hergenröder, R., Samek, O., Hommes, V., 2006. Femtosecond laser ablation elemental mass spectrometry. Mass Spectrom. Rev. 25 (4), 551–572.

Hirata, T., Kon, Y., 2008. Evaluation of the analytical capability of NIR femtosecond laser ablation-inductively coupled plasma mass spectrometry. Anal. Sci. 24 (3), 345–353.

Horn, I., von Blanckenburg, F., 2007. Investigation on elemental and isotopic fractionation during 196 nm femtosecond laser ablation multiple collector inductively coupled plasma mass spectrometry. Spectrochim. Acta B At. Spectrosc. 62 (4), 410–422.

Horn, I., von Blanckenburg, F., Schoenberg, R., Steinhoefel, G., Markl, G., 2006. In situ iron isotope ratio determination using UV-femtosecond laser ablation with application to hydrothermal ore formation processes. Geochim. Cosmochim. Acta 70 (14), 3677–3688.

Horstwood, M.S.A., Evans, J.A., Montgomery, J., 2008. Determination of Sr isotopes in calcium phosphates using laser ablation inductively coupled plasma mass spectrometry and their application to archaeological tooth enamel. Geochim. Cosmochim. Acta 72 (23), 5659–5674.

Hu, Z.C., Gao, S., Liu, Y.S., Hu, S.H., Chen, H.H., Yuan, H.L., 2008. Signal enhancement in laser ablation ICP-MS by addition of nitrogen in the central channel gas. J. Anal. At. Spectrom. 23 (8), 1093–1101.

Hu, Z.C., Liu, Y.S., Gao, S., Liu, W.G., Zhang, W., Tong, X.R., Lin, L., Zong, K.Q., Li, M., Chen, H.H., Zhou, L., Yang, L., 2012a. Improved in situ Hf isotope ratio analysis of zircon using newly designed X skimmer cone and jet sample cone in combination with the addition of nitrogen by laser ablation multiple collector ICP-MS. J. Anal. At. Spectrom. 27 (9), 1391–1399.

Hu, Z.C., Liu, Y.S., Gao, S., Xiao, S.Q., Zhao, L.S., Günther, D., Li, M., Zhang, W., Zong, K.Q., 2012b. A "wire" signal smoothing device for laser ablation inductively coupled plasma mass spectrometry analysis. Spectrochim. Acta B At. Spectrosc. 78 (0), 50–57.

Ikehata, K., Hirata, T., 2013. Evaluation of UV-fs-LA-MC-ICP-MS for precise in situ copper isotopic microanalysis of cubanite. Anal. Sci. 29 (12), 1213–1217.

Ikehata, K., Notsu, K., Hirata, T., 2008. In situ determination of Cu isotope ratios in copper-rich materials by NIR femtosecond LA-MC-ICP-MS. J. Anal. At. Spectrom. 23 (7), 1003–1008.

Jackson, M.G., Hart, S.R., 2006. Strontium isotopes in melt inclusions from Samoan basalts: implications for heterogeneity in the Samoan plume. Earth Planet. Sci. Lett. 245 (1–2), 260–277.

Jochum, K.P., Stoll, B., Weis, U., Kuzmin, D.V., Sobolev, A.V., 2009. In situ Sr isotopic analysis of low Sr silicates using LA-ICP-MS. J. Anal. At. Spectrom. 24 (9), 1237–1243.

Jochum, K.P., Stoll, B., Weis, U., Jacob, D.E., Mertz-Kraus, R., Andreae, M.O., 2014. Non-matrix-matched calibration for the multi-element analysis of geological and environmental samples using 200 nm femtosecond LA-ICP-MS: a comparison with nanosecond lasers. Geostand. Geoanal. Res. 38 (3), 265–292.

Kimura, J., Takahashi, T., Chang, Q., 2013. A new analytical bias correction for in situ Sr isotope analysis of plagioclase crystals using laser-ablation multiple-collector inductively coupled plasma mass spectrometry. J. Anal. At. Spectrom. 28 (6), 945–957.

Kimura, J., Chang, Q., Itano, K., Iizuka, T., Vaglarov, B.S., Tani, K., 2014. An improved U-Pb age dating method for zircon and monazite using 200/266 nm femtosecond laser ablation and enhanced sensitivity multiple-Faraday collector inductively-coupled plasma mass spectrometry. J. Anal. At. Spectrom. 30 (2), 494–505.

Koch, J., Wälle, M., Pisonero, J., Günther, D., 2006. Performance characteristics of ultraviolet femtosecond laser ablation inductively coupled plasma mass spectrometry at 265 and 200 nm. J. Anal. At. Spectrom. 21 (9), 932–940.

Koornneef, J.M., Nikogosian, I., van Bergen, M.J., Smeets, R., Bouman, C., Davies, G.R., 2015. TIMS analysis of Sr and Nd isotopes in melt inclusions from Italian potassium-rich lavas using prototype 1013 Ω amplifiers. Chem. Geol. 397, 14–23.

Li, Z., Hu, Z.C., Liu, Y.S., Gao, S., Li, M., Zong, K.Q., Chen, H.H., Hu, S.H., 2015. Accurate determination of elements in silicate glass by nanosecond and femtosecond laser ablation ICP-MS at high spatial resolution. Chem. Geol. 400, 11–23.

Li, Z., Hu, Z.C., Günther, D., Zong, K.Q., Liu, Y.S., Luo, T., Zhang, W., Gao, S., Hu, S.H., 2016. Ablation characteristic of ilmenite using UV nanosecond and femtosecond lasers: implications for non-matrix-matched quantification. Geostand. Geoanal. Res. 40 (4), 477–491.

Lin, L., Hu, Z.C., Yang, L., Zhang, W., Liu, Y.S., Gao, S., Hu, S.H., 2014. Determination of boron isotope compositions of geological materials by laser ablation MC-ICP-MS using newly designed high sensitivity skimmer and sample cones. Chem. Geol. 386 (0), 22–30.

von der Linde, D., Sokolowski-Tinten, K., Bialkowski, J., 1997. Laser–solid interaction in the femtosecond time regime. Appl. Surf. Sci. 109–110, 1–10.

Liu, X., Du, D., Mourou, G., 1997. Laser ablation and micromachining with ultrashort laser pulses. IEEE J. Quantum Elect. 33 (10), 1706–1716.

Liu, S.H., Hu, Z.C., Gunther, D., Ye, Y.H., Liu, Y.S., Gao, S., Hu, S.H., 2014. Signal enhancement in laser ablation inductively coupled plasma-mass spectrometry using water and/or ethanol vapor in combination with a shielded torch. J. Anal. At. Spectrom. 29 (3), 536–544.

Mao, S.S., Quéré, F., Guizard, S., Mao, X., Russo, R.E., Petite, G., Martin, P., 2004. Dynamics of femtosecond laser interactions with dielectrics. Appl. Phys. A-Mater 79 (7), 1695–1709.

Oeser, M., Weyer, S., Horn, I., Schuth, S., 2014. High-precision Fe and Mg isotope ratios of silicate reference glasses determined in situ by femtosecond LA-MC-ICP-MS and by solution nebulisation MC-ICP-MS. Geostand. Geoanal. Res. 38 (3), 311–328.

Ohata, M., Nonose, N., Dorta, L., Günther, D., 2015. Comparison of 265 nm femtosecond and 213 nm nanosecond laser ablation inductively coupled plasma mass spectrometry for Pb isotope ratio measurements. Anal. Sci. 31 (12), 1309–1315.

Outridge, P., Chenery, S., Babaluk, J., Reist, J., 2002. Analysis of geological Sr isotope markers in fish otoliths with subannual resolution using laser ablation-multicollector-ICP-mass spectrometry. Environ. Geol. 42 (8), 891–899.

Pisonero, J., Günther, D., 2008. Femtosecond laser ablation inductively coupled plasma mass spectrometry: fundamentals and capabilities for depth profiling analysis. Mass Spectrom. Rev. 27 (6), 609–623.

Poitrasson, F., Mao, X., Mao, S.S., Freydier, R., Russo, R.E., 2003. Comparison of ultraviolet femtosecond and nanosecond laser ablation inductively coupled plasma mass spectrometry analysis in glass, monazite, and zircon. Anal. Chem. 75 (22), 6184–6190.

Ramos, F.C., Tepley, F.J., 2008. Inter- and intracrystalline isotopic disequilibria: techniques and applications. Rev. Mineral. Geochem. 69 (1), 403–443.

Ramos, F.C., Wolff, J.A., Tollstrup, D.L., 2004. Measuring 87Sr/86Sr variations in minerals and groundmass from basalts using LA-MC-ICPMS. Chem. Geol. 211 (1–2), 135–158.

Russell, W.A., Papanastassiou, D.A., Tombrello, T.A., 1978. Ca isotope fractionation on the earth and other solar system materials. Geochim. Cosmochim. Acta 42 (8), 1075–1090.

Russo, R.E., Mao, X.L., Gonzalez, J.J., Mao, S.S., 2002. Femtosecond laser ablation ICP-MS. J. Anal. At. Spectrom. 17 (17), 1072–1075.

Schmidberger, S.S., Simonetti, A., Francis, D., 2003. Small-scale Sr isotope investigation of clinopyroxenes from peridotite xenoliths by laser ablation MC-ICP-MS—implications for mantle metasomatism. Chem. Geol. 199 (3–4), 317–329.

Schuessler, J.A., von Blanckenburg, F., 2014. Testing the limits of micro-scale analyses of Si stable isotopes by femtosecond laser ablation multicollector inductively coupled plasma mass spectrometry with application to rock weathering. Spectrochim. Acta B At. Spectrosc. 98, 1–18.

Shaheen, M., Fryer, B.J., 2010. Improving the analytical capabilities of femtosecond laser ablation multicollector ICP-MS for high precision Pb isotopic analysis: the role of hydrogen and nitrogen. J. Anal. At. Spectrom. 25 (7), 1006–1013.

Shaheen, M.E., Gagnon, J.E., Fryer, B.J., 2012. Femtosecond (fs) lasers coupled with modern ICP-MS instruments provide new and improved potential for in situ elemental and isotopic analyses in the geosciences. Chem. Geol. 330, 260–273.

Steinhoefel, G., Horn, I., von Blanckenburg, F., 2009a. Matrix-independent Fe isotope ratio determination in silicates using UV femtosecond laser ablation. Chem. Geol. 268 (1–2), 67–73.

Steinhoefel, G., Horn, I., von Blanckenburg, F., 2009b. Micro-scale tracing of Fe and Si isotope signatures in banded iron formation using femtosecond laser ablation. Geochim. Cosmochim. Acta 73 (18), 5343–5360.

Steinhoefel, G., Breuer, J., von Blanckenburg, F., Horn, I., Kaczorek, D., Sommer, M., 2011. Micrometer silicon isotope diagnostics of soils by UV femtosecond laser ablation. Chem. Geol. 286 (3–4), 280–289.

Tong, X.R., Liu, Y.S., Hu, Z.C., Chen, H.H., Zhou, L., Hu, Q.H., Xu, R., Deng, L.X., Chen, C.F., Yang, L., Gao, S., 2016. Accurate determination of Sr isotopic compositions in clinopyroxene and silicate glasses by LA-MC-ICP-MS. Geostand. Geoanal. Res. 40 (1), 85–99.

Vroon, P.Z., Wagt, B.V.D., Koornneef, J.M., Davies, G.R., 2008. Problems in obtaining precise and accurate Sr isotope analysis from geological materials using laser ablation MC-ICPMS. Anal. Bioanal. Chem. 390 (2), 65–76.

Waight, T., Baker, J., Peate, D., 2002. Sr isotope ratio measurements by double-focusing MC-ICPMS: techniques, observations and pitfalls. Int. J. Mass Spectrom. 221 (3), 229–244.

Woodhead, J., Swearer, S., Hergt, J., Maas, R., 2005. In situ Sr-isotope analysis of carbonates by LA-MC-ICP-MS: interference corrections, high spatial resolution and an example from otolith studies. J. Anal. At. Spectrom. 20 (1), 22–27.

Wu, T., Xiao, L., Wilde, S.A., Ma, C.Q., Li, Z.L., Sun, Y., Zhan, Q.Y., 2016. Zircon U–Pb age and Sr–Nd–Hf isotope geochemistry of the Ganluogou dioritic complex in the northern Triassic Yidun arc belt, Eastern Tibetan Plateau: implications for the closure of the Garzê-Litang Ocean. Lithos 248–251, 94–108.

Xu, L., Hu, Z.C., Zhang, W., Yang, L., Liu, Y.S., Gao, S., Luo, T., Hu, S.H., 2015. In situ Nd isotope analyses in geological materials with signal enhancement and non-linear mass dependent fractionation reduction using laser ablation MC-ICP-MS. J. Anal. At. Spectrom. 30 (1), 232–244.

Yang, Y.H., Wu, F.Y., Wilde, S.A., Liu, X.M., Zhang, Y.B., Xie, L.W., Yang, J.H., 2009. In situ perovskite Sr–Nd isotopic constraints on the petrogenesis of the Ordovician Mengyin kimberlites in the North China Craton. Chem. Geol. 264 (1–4), 24–42.

Yang, Y.H., Zhang, H.F., Chu, Z.Y., Xie, L.W., Wu, F.Y., 2010. Combined chemical separation of Lu, Hf, Rb, Sr, Sm and Nd from a single rock digest and precise and accurate isotope determinations of Lu–Hf, Rb–Sr and Sm–Nd isotope systems using multi-collector ICP-MS and TIMS. Int. J. Mass Spectrom. 290 (2–3), 120–126.

Yang, Y.H., Wu, F.Y., Xie, L.W., Yang, J.H., Zhang, Y.B., 2011a. High-precision direct determination of the 87Sr/86 Sr isotope ratio of bottled Sr-rich natural mineral drinking water using multiple collector inductively coupled plasma mass spectrometry. Spectrochim. Acta B At. Spectrosc. 66 (8), 656–660.

Yang, Z.P., Fryer, B.J., Longerich, H.P., Gagnon, J.E., Samson, I.M., 2011b. 785 nm femtosecond laser ablation for improved precision and reduction of interferences in Sr isotope analyses using MC-ICP-MS. J. Anal. At. Spectrom. 26 (2), 341–351.

Yang, Y.H., Wu, F.Y., Xie, L.W., Chu, Z.Y., Yang, J.H., 2014. Re-evaluation of interferences of doubly charged ions of heavy rare earth elements on Sr isotopic analysis using multi-collector inductively coupled plasma mass spectrometry. Spectrochim. Acta B At. Spectrosc. 97, 118–123.

Zhang, W., Hu, Z., Yang, L., Liu, Y., Zong, K., Xu, H., Chen, H., Gao, S., Xu, L., 2015. Improved inter-calibration of faraday cup and ion counting for in situ Pb isotope measurements using LA-MC-ICP-MS: application to the study of the origin of the Fangshan pluton, North China. Geostand. Geoanal. Res. 39 (4), 467–487.

Zhang, W., Hu, Z., Günther, D., Liu, Y., Ling, W., Zong, K., Chen, H., Gao, S., 2016. Direct lead isotope analysis in Hg-rich sulfides by LA-MC-ICP-MS with a gas exchange device and matrix-matched calibration. Anal. Chim. Acta 948, 9–18.